INSTITUTE OF PHYSICS PUBLISHING JOURNAL OF PHYSICS: CONDENSED MATTER

J. Phys.: Condens. Matter **18** (2006) S2543–S2561 doi:10.1088/0953-8984/18/38/S02

Surface engineering of Co and FeCo nanoparticles for biomedical application

Silke Behrens[1], Helmut Bönnemann[1,3], Nina Matoussevitch[1,2], Angelika Gorschinski[1], Eckhard Dinjus[1,2], Wilhelm Habicht[1], Jens Bolle[4], Svetlana Zinoveva[5], Natalie Palina[5], Josef Hormes[5], Hartwig Modrow[5], Stephan Bahr[6] and Volker Kempter[6]

[1] Institut für Technische Chemie, Bereich Chemisch-Physikalische-Verfahren, Forschungszentrum Karlsruhe, Postfach 3640, 76021 Karlsruhe, Germany
[2] Universität Heidelberg, Im Neuenheimer Feld 253, 69117 Heidelberg, Germany
[3] Max-Planck-Institut für Kohlenforschung, Kaiser-Wilhelm-Platz 1, 45470 Mülheim, Germany
[4] Institut für Technische Chemie, Bereich Wasser-Geotechnologie, Forschungszentrum Karlsruhe, Postfach 3640, 76021 Karlsruhe, Germany
[5] Physikalisches Institut, Universität Bonn, Nußallee 12-14, D-53115 Bonn, Germany
[6] Institut für Physik und Physikalische Technologien, TU Clausthal, 38678 Clausthal-Zellerfeld, Germany

E-mail: silke.behrens@itc-cpv.fzk.de

Received 15 May 2006, in final form 6 July 2006
Published 8 September 2006
Online at stacks.iop.org/JPhysCM/18/S2543

Abstract

Monodisperse Co, Fe, and FeCo nanoparticles are prepared via thermal decomposition of metal carbonyls in the presence of aluminium alkyls, yielding air-stable magnetic metal nanoparticles after surface passivation. The particles are characterized by electron microscopy (SEM, TEM, ESI), electron spectroscopy (MIES, UPS, and XPS) and x-ray absorption spectroscopy (EXAFS). The particles are peptized by surfactants to form stable magnetic fluids in various organic media and water, exhibiting a high volume concentration and a high saturation magnetization. In view of potential biomedical applications of the particles, several procedures for surface modification are presented, including peptization by functional organic molecules, silanization, and *in situ* polymerization.

1. Introduction

Originally, magnetic fluids (MFs) [1] were produced by grinding ferrites in a carrier liquid, for example, in heptane or long chain alkyls in the presence of a suitable surfactant, usually oleic acid, until the ferrite was in a colloidal state [2]. Later procedures for MFs precipitated magnetite from an aqueous Fe^{2+}/Fe^{3+} solution with a base, coated the particles by a surfactant, and dispersed them into a non-polar carrier liquid [3]. Water-based MFs could be prepared,

for example, from magnetite particles coated by oleic acid as a first lipophilic layer, followed by forming a second hydrophilic surfactant layer with an anionic or nonionic surfactant. Since then, the field of MFs has quickly developed in terms of MF preparation, characterization and fundamental description, as well as their technical and biomedical application. MFs reveal interesting properties for technical applications, including high vacuum seals, bearings, brakes, dampers, and positioning systems [4]. Moreover, superparamagnetic iron oxide particles with appropriate surface chemistry have been used for numerous *in vivo* and *in vitro* applications, for example, magnetic resonance imaging (MRI), hyperthermia, drug delivery, magnetofection, or cell separation [5–8]. Usually, these applications need a special surface coating, which has to be, for example, biocompatible or allows specific targeting for drug delivery or cell separation. The engineering of particle surfaces by organic (polymer) and inorganic (metal or oxide) coatings suitable for further functionalization with bioactive molecules has been reported [9, 5, 10]. Besides the elemental composition, the surface and crystal structure of the particles, particle size and particle size distribution strongly influence the properties of the magnetic particles and resulting MFs.

There are two major advantages of using MFs based on magnetic metal or alloy particles, for example, Co, Fe, or FeCo particles. Firstly, these metals exhibit a high magnetization saturation, and secondly, they can be produced with a narrow size distribution. However, they usually oxidize easily in the presence of air and, thus, subsequently lose their magnetic properties, a fact restricting application. A number of methods for producing small magnetic metal particles have been reported in the literature. Usually, a metal carbonyl is decomposed in the presence of a stabilizing ligand such as oleic acid or oleyl amine. Co [11–17], Fe [18–20], and FeCo [21, 22] nanoparticles, for example, were synthesized from $Co_2(CO)_8$ and $Fe(CO)_5$ precursors.

We address the synthesis of air-stable metallic Co, Fe, and FeCo particles by decomposition of the corresponding metal carbonyl precursors in the presence of aluminium alkyls. The particles can be peptized by appropriate surfactants in various non-polar carrier liquids, ethanol, and water, resulting in remarkably stable MFs with a high magnetization saturation. Moreover, several procedures have been developed in order to design an appropriate surface chemistry for potential biomedical applications, including peptization by functional organic molecules, silanization, and *in situ* polymerization.

2. Experiment

2.1. Synthesis of metallic and alloyed Co, Fe, and FeCo nanoparticles

All procedures for particle synthesis were carried out under argon atmosphere using dry solvents. Co nanoparticles were synthesized as described elsewhere [23]. Briefly, 171 g $Co_2(CO)_8$ were added to $Al(C_8H_{17})_3$ in 3000 ml toluene and heated at 110 °C for 18 h, then for 2 h at 150 °C under stirring. After cooling the reaction mixture to room temperature, the particles were smoothly oxidized by synthetic air, which was introduced through a thin capillary. The resulting black precipitate was washed two times with 1500 ml toluene. The precipitate was allowed to settle, the supernatant was decanted, and the Co particles were isolated as a suspension in 100 ml toluene. Fe and FeCo nanoparticles were synthesized according to [24]. For a typical synthesis, 50 g $Fe(CO)_5$ (255.2 mM) and 21.81 g $Co_2(CO)_8$ (63.8 mM) were stirred in 500 ml tetrahydronaphthalene at room temperature for 3 days. After adding 20.3 ml $Al(C_8H_{17})_3$ (38.4 mM), the reaction mixture was heated slowly to 90 °C, followed by stepwise heating at 10 °C h^{-1} to 120 °C releasing CO. The temperature was carefully raised to 150 °C to finalize the gas evolution. *Smooth oxidation* (*pre-stabilization*)

of the nanoparticles was performed by applying oxygen (3.5 vol% O_2 in argon) through a thin capillary. After washing with toluene, the precipitate was isolated as a suspension in 100 ml toluene.

2.2. Preparation of MFs

The particles were peptized with KorantinSH (N-oleyl sarcosine, BASF AG), AOT (sodium dioctyl sulfosuccinate, SERVA2), and LP4 (fatty acid condensation polymer, ICI Ltd) to obtain MFs in various non-polar carrier liquids as described in [23, 24]. For preparing water-based MFs, particles were coated by surfactant double layers of KorantinSH, oleic acid, or oleylamine as a first hydrophobic layer and dodecylsulfate as a second hydrophilic layer or by using tetramethylammonium hydroxide as a phase transfer agent as described in detail in [25].

2.3. Surface modification for biomedical applications

2.3.1. L-cysteine ethyl ester. Particles were functionalized with L-cysteine ethyl ester according to a procedure reported in [25]. Briefly, 0.5 g Co nanoparticles (synthesis see above) were washed sincerely with ethanol, followed by washing with water. The particles were then peptized in 10 ml aqueous L-cysteine ethyl ester solution (2% L-cysteine ethyl ester in water). Fe/Co particles were also peptized using L-cysteine ethyl ester in water and applying a similar procedure.

2.3.2. Dextran coating. 0.5 g Co nanoparticles modified with L-cysteine ethyl ester were suspended in 10 ml ethanol containing 0.5 g dextran (molecular weight 10 000) or carbomethoxydextran (CMD). The reaction mixture was heated at 30 °C for 20 min and kept for 24 h at room temperature under shaking. The dextran coated particles were washed several times with ethanol. Dextran coating could be also performed on unpeptized Co nanoparticles: a suspension of Co particles (containing 2 g cobalt) in 25 ml 0.5 M NaOH was slowly added to 2 g dextran (or CMD) in 25 ml 0.5 M NaOH. The reaction mixture was heated at 30 °C for 30 min and kept for 24 h at room temperature under shaking. The dextran coated particles were washed several times. The coated particles were either suspended in water or ethanol or used in a dried form.

These procedures were also applied for dextran coating of FeCo particles.

2.3.3. SiO_2 coating. Procedures for SiO_2 coating were carried out under argon atmosphere. Typically, 3 g Co nanoparticles were peptized with oleic acid in 180 ml toluene. 600 μl NH_4OH in 18 ml ethanol and 3 ml tetraethoxysilane (TEOS) were added, and the mixture was stirred overnight at room temperature, and finally heated at 110 °C for 1 h (sample Co@SiO_2-1). After washing the particles extensively with ethanol, they were redispersed in ethanol. For unpeptized particles, 1 ml Co suspension (0.67 g Co) was diluted to 270 ml with toluene. After sonicating the suspension for 1 h, 5.5 ml TEOS were added (sample Co@SiO_2-2). The reaction mixture was stirred at room temperature for 1 h, followed by heating at 110 °C for 1 h. After washing the particles extensively with ethanol, they were redispersed in ethanol.

Co or Fe containing SiO_2 microspheres were prepared by a two-step procedure: 25 ml of a suspension of Co nanoparticles in toluene (0.5 g Co) were firstly washed with ethanol and water and suspended in 10 ml water. 12 ml APS (40 μl APS in 12 ml water) were added and the mixture was sonicated (15 min). 30 ml active silica (1.2 g natron water glass in 200 ml water) were added and the mixture was stirred for 24 h at room temperature. The product was separated and washed with water. Secondly, the particles were suspended in 20 ml

water/ethanol (1:4), 1.2 ml TEOS and 4 ml NH_4OH were added to the reaction mixture, which was stirred for 24 h at room temperature. The product was washed with ethanol.

2.3.4. Polymer microspheres. Magnetic poly(methylmetacrylate-divinylbenzene) microspheres were prepared by suspension polymerization: the oil phase was composed of 5 g Co nanoparticles coated by KorantinSH in 30 ml dichlormethane/hexane (1:1), 90 ml methyl metacrylate (MMA), 10 ml divinylbenzene (DVB), and 2 g benzoyl peroxide (BPO) as an initiator. 25 g polyvinylalcohol (PVA) as stabilizer and 25 g NaCl were dissolved in 1500 ml water at 60 °C and a few ml methylene blue were added. The oil phase was added to the aqueous solution under vigorous stirring (800–1000 rpm) under N_2 atmosphere. After 1 h the emulsion was heated to 80 °C for 4 h. The poly(MMA-DVB) microspheres were separated from the reaction mixture and washed several times with deionized water. The resulting microspheres were finally fractioned by sedimentation.

2.4. Electron microscopy

Transmission electron microscopy (TEM), high-resolution TEM (HRTEM), and selected area electron diffraction (SAED) were performed using a Philips Tecnai F20 TEM with field emission gun at 200 kV equipped with EDX and a Gatan imaging filter for energy-filtered TEM (EFTEM). Typically, a 20 μl droplet of the sample was placed on a carbon coated, 400 mesh copper grid, and air dried. Elemental maps of Co, Si, and O were acquired using the three-window technique. Scanning electron microscopy (SEM) analysis was made using a LEO Gemini 982 scanning electron microscope (SEM) equipped with a LINK ISIS 300 energy-dispersive x-ray (EDX) analysis unit from Oxford Corp.

2.5. Magnetic measurements

Magnetic measurements of $Co@SiO_2$ particles and poly(MMA-DVB) microspheres were performed with a Micro Mag alternating gradient magnetometer (AGM) from Princeton Measurement Corp. on the dried powders at room temperature.

2.6. Electron spectroscopy

A combination of metastable impact electron spectroscopy (MIES) and photoelectron spectroscopy, UPS(HeI) and XPS, was applied to provide information on the chemical properties and the electronic structure of the outermost layer as well as on the surface-near region of the particles.

In MIES, metastable He atoms are utilized to eject electrons from surfaces. He^* metastables (in the 2^3S state mainly) of thermal energy interact via Auger processes with condensed matter, including nanoparticles, depending on the electronic structure of the surface under consideration and its work function [26–30]. While the energy balance of MIES (at least for the auger deexcitation (AD) process) is quite similar to that for photoelectron spectroscopy (UPS) (HeI), the depth information of MIES is *zero* because the Auger processes, Auger deexcitation (AD) under the present conditions, typically take place 4 Å in front of the surface, and electrons are ejected from species of the outermost layer of the nanoparticles. On the other hand, the depth information of UPS (HeI) is about 3 monolayers (ML), i.e. this technique provides information on the near-surface region, although averaged over 3 ML. In MIES the number of electrons emitted in an AD process is, to a good approximation, proportional to the density of the states involved in the emission process. Thus, MIES spectra image the electronic

structure of the surface under study. On the other hand, UPS with HeI radiation provides the electronic structure averaged over about 3 layers.

The apparatus is, in addition, equipped with a twin anode (Mg/Al) XPS source for the characterization of the chemical composition of the bare surface as well as of films via core level spectroscopy. These core level spectra depend on the chemical environment of the atoms which are ionized. In the present work, the chemical shift of 2p Co and 2p Fe emission will be utilized to obtain information on the eventual oxidation of the MFs.

2.7. X-ray absorption spectroscopy

XANES spectra were collected at the XMP beamline at the 1.3 GeV electron storage ring at the CAMD. Details of this beamline can be found in the literature [31]. The experiments were done in transmission mode using ionization chambers as detectors. As filling gas, 50 mbar helium was used for S K-edge measurements and 1 atm air for measurements at the Co K-edge, respectively. The Lemonnier-type monochromator [32] was equipped with Ge 220 crystals, and the photon energy was calibrated relative to the absorption spectrum of a cobalt foil setting to the first inflection point at 7709 eV for the Co K-edge [33]. In contrast, In Sb 111 crystals were used for measurements at the S K-edge, where the photon energy was calibrated relative to the first maximum of a $ZnSO_4$ spectrum, which was assigned an energy value of 2481.44 eV. The sample preparation, the parameter control for XAS measurements, and the data collection modes were set as suggested by the guidelines of the International XAFS Society Standards and Criteria Committee [34, 35]. Major experimental issues were the following: XANES spectra were scanned with −100, −20, 40, and 200 eV intervals relative to the Co K-edge and a step width of 2, 0.4, and 1 eV per respective interval and with 2440, 2468, 2484, and 2510 eV intervals for the S K-edge with respective step width of 0.5, 0.1, and 0.3 eV. The XANES spectra were averaged over three scans with an integration time of 1000 ms. Standard XANES data analysis, consisting of linear background subtraction and spectra normalization to an absorption of 1 at 7797 eV photon energy for Co K-edge data and 2498 eV for S K-edge data, respectively, was performed using the WINXAS97 software package [36].

3. Results and discussion

3.1. Synthesis of metal nanoparticles and preparation of MFs

Monodisperse magnetic Co nanoparticles were obtained via thermal decomposition of $Co_2(CO)_8$ in the presence of aluminium alkyls (AlR_3, R = alkyl) [23]. Thereafter, the metal particles were treated carefully with synthetic air through a thin capillary (*smooth oxidation*), yielding particles stable in air under ambient conditions for over one year, as confirmed by magnetic measurements. The surface stabilization occurs stepwise via the oxidation of residual CO at the metal surface. If the surface remained unpassivated by *smooth oxidation*, the saturation magnetization decreased rapidly when exposed to air.

$$Co_2(CO)_8 + AlR_3 \xrightarrow[\text{(2) synthetic air}]{\text{(1) 110 °C, toluene}} \text{Co(0) nanoparticles with an oxidized protecting shell.}$$

The aluminium alkyl acts as a catalyst, activating the thermal decomposition of the metal carbonyl as well as the surface passivation during *smooth oxidation*. The resulting particles strongly depend on the applied reaction parameters, namely the alkyl chain length R of the aluminium alkyl and the $Co_2(CO)_8$ to AlR_3 ratio. Monodisperse Co nanoparticles, 3–4.5 nm, 6.5–8.5 nm to 8.5–10.5 nm in diameter, were obtained for $Al(CH_3)_3$, $Al(C_2H_5)_3$, and $Al(C_8H_{17})_3$, respectively. Molar Co:Al ratios of 10:1 and 1:2 yielded particle diameters of

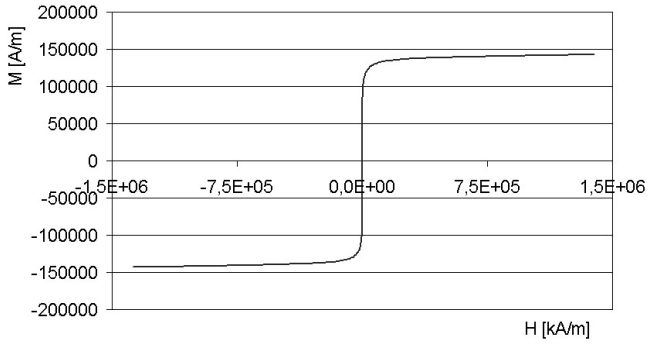

Figure 1. Magnetization curve of a Co MF in mineral oil WT12.

10 ± 1.1 and 5 ± 1.1 nm. It should be noted that this type of modification can also have measurable impact on the structural properties of nanoscaled particles, as discussed in detail in previous publications on this [41, 25] and other [37–39] systems.

The *pre-stabilized* particles could be peptized by suitable surfactants, resulting in MFs which were remarkably stable and which showed a high magnetization saturation (>170 mT) and high volume concentration (e.g. 10 vol% Co). Various surfactants, for example, KorantinSH (N-oleyl sarcosine), AOT (sodium dioctyl sulfosuccinate), and LP4 (fatty acid condensation polymer) were used to prepare MFs in unpolar organic carrier liquids such as kerosene, vacuum and mineral oil. Figure 1 displays an example for a magnetization curve of an MF of Co particles peptized with KorantinSH/LP4 in mineral oil WT12. For further examples see also [25]. Some of these MFs have already been tested successfully for technical application [25]. Water-based MFs were obtained via the formation of bi- or polylayers around the air-stable particles by using ionic, non-ionic, or double surfactants. Usually, oleic acid or KorantinSH were applied forming a first lipophilic layer, followed by addition of sodium oleate, sodium dodecylsulfonate, or dodecylamine resulting in a second hydrophilic layer. Alternatively, water-based MFs were obtained via phase-transfer using tetramethylammoniumhydroxide.

The peptized particles exhibit a structure consisting of a metallic Co core, a protective oxide shell, and an outer layer formed by the surfactant. EXAFS analysis on Co-based MFs suggests that Co–C coordination resulting after *smooth oxidation* from oxidized surface carbonyls might be substituted by Co–O coordination which may be attributed to the coordination of the carboxyl functionality of oleic acid to the particle surface. It should be stressed that the nature of the shell is highly sensitive to the reaction parameters which have been applied [40]. The particle core consists of metallic Co exhibiting a face centred cubic (fcc) or hexagonal close-packed (hcp) Co structure, depending on the synthetic procedure applied. TEM analysis reveals the monodisperse nature of the peptized Co nanoparticles (figure 2(a)). TEM images indicated that the protecting oxide layer was very thin. Figures 2(b) and (c) display the results of energy-filtered TEM (EFTEM) taken using the Co $L_{2,3}$ and the O K edge. The bright contrast in figure 2 represents Co (b) and O (c), respectively.

Similar to the controlled thermolysis of $Co_2(CO)_8$, Fe or FeCo nanoparticles were produced via thermal decomposition of $Fe(CO)_5$ and $Fe(CO)_5/Co_2(CO)_8$ in the presence of aluminium alkyls. For further details see [24].

Electron spectroscopy, combining MIES, UPS and XPS, was utilized to gather information on the composition and the electronic structure of the particle shell. The following strategy has been pursued for Co nanoparticles [25].

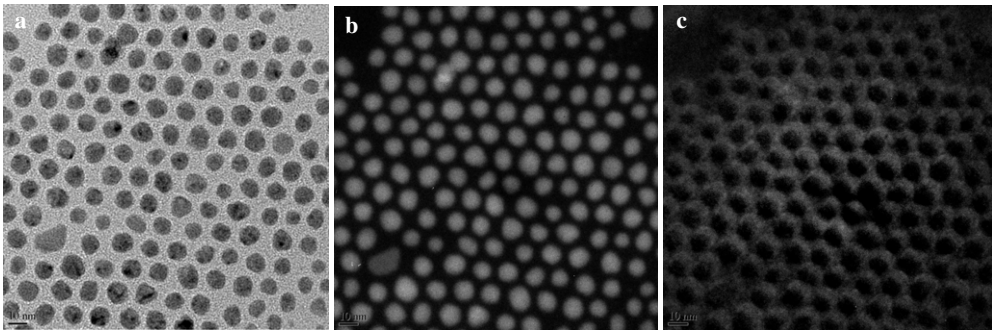

Figure 2. (a) TEM image showing monodisperse Co nanoparticles peptized by oleic acid. EFTEM images of the peptized Co nanoparticles: elemental maps of the Co $L_{2,3}$ edge (b) and the O K edge (c).

(1) In a first step, a planar Co film is studied with MIES and UPS, eventually supported by techniques that give additional information on the chemical composition of the metal film prior to and after being subjected to the shell molecules (XPS) and on the film topology (STM). Then, the interaction of selected atomic and/or molecular species (*shell molecules*) (see below) with this film has to be studied in the same way. This step yields *fingerprint spectra* providing structural information on the Co film surface, neat and covered by the molecules that potentially form the shell of the nanoparticles.

(2) In a second step, the corresponding analysis is performed on the Co nanoparticles, usually possessing a shell which results from wet-chemical procedures. An obvious complication arises from the fact that the composition of the shell produced in this way is *a priori* unknown, i.e. normally cannot be predicted on the basis of the performed wet-chemical procedures alone. A comparison of the results from step (2) with a series of *fingerprint spectra* is required which have either been gathered in step (1) or are already available in the literature. The *pre-stabilized* Co particles were deposited on SiO_x substrates from suspensions in toluene [41]. STM indicated that a closed layer of the particles was obtained. Heating was required to remove surface contaminations that apparently originate from residual solvent molecules. Although the results obtained for oxygen-exposed planar Co films do not allow for a unique identification of the species terminating the particles surface, it appears safe to state that the formation of both (Co–O) and (Co–CO_x) bonds is responsible for the *pre-stabilization* of the Co nanoparticle surface which persists up to about 250 °C. We estimated that most of the intensity observed in the valence band region (about 70%) is due to (Co–CO_x)-, not due to (Co–O)-bonds. Detailed information is available on the oxidation kinetics of ultra-thin Co films [42]. It was shown that Co films of a thickness larger than 5 nm, deposited on oxidized Si(111), oxidize instantaneously whereby a thickness of 2.5 nm of the Co metal is transformed into oxide. On the other hand, the time constant for oxidation increases linearly for thinner films due to the change of the magnetic properties under the influence of the substrate. It reaches about 100 days for 2.5 nm, indicating that products other than CoO are likely to be formed in this region. Thus, detailed additional studies are still required in order to elucidate the kinetics for the formation of the passivating layer formed on the Co particles by *smooth oxidation*.

3.2. Surface modification for biomedical applications

One of the challenges to application in various areas, for example, in biomedical systems as well as medical therapy and diagnosis, lies in the engineering of a robust, tailored surface functionality ensuring biocompatibility and allowing specific site targeting. Several methods

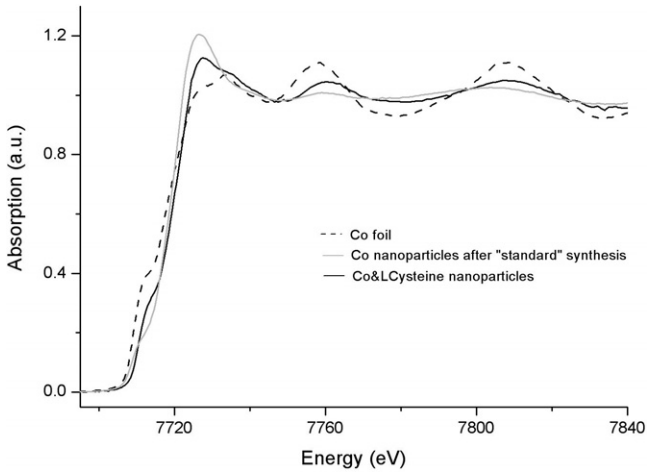

Figure 3. Co K-edge XANES spectra of Co nanoparticles peptized by L-cysteine ethyl ester (black solid line) in comparison with Co foil (black dashed line) and Co nanoparticles (grey solid line).

have been developed to modify the surface properties of the magnetic Co and FeCo particles, suitable for attachment of functional, bioactive groups, for example, by peptization with functional organic molecules, silanization, and *in situ* polymerization.

3.2.1. Surface functionalization by L-cysteine ethyl ester. Co and FeCo particles can be peptized by L-cysteine ethyl ester in water and ethanol. The particles were peptized by the thiol group of L-cysteine ethyl ester with the amino acid remaining free, which was confirmed by infrared spectra [25]. Naturally, it is of special interest to analyse what effects are induced by this modification to the structure and properties of the particle, as in general surface modification has been shown to have a notable influence on the electronic structure and magnetic properties of such particles [43–47]. Co K-edge XANES spectra of the thus modified Co nanoparticles, a spectrum of Co foil and Co nanoparticles after 'standard' synthesis are shown in figure 3. The pre-edge intensity is reasonably close to that for metallic cobalt. Together with the absence of drastically increased white line intensity and the presence of only one broad resonance at 7773 eV in the spectra of cobalt oxide which were not observed for the Co nanoparticles, this indicates that one is still dealing with metallic particles which are not oxidized, implying some degree of protection of the cobalt core. The small change in white line intensity relative to an hcp Co foil can be attributed to the presence of an fcc rather than an hcp core, as discussed in detail for example in [48]. There is, however, one clear deviation from the spectra of both reference foil and Co nanoparticles obtained using an identical procedure, but without L-cysteine ethyl ester as peptization agent, which are also shown in figure 3: there is a slight chemical shift of the absorption edge towards slightly higher energy and a slight increase in the energy position of the shape resonance at 7760 eV. Tentatively, bearing in mind the importance of surface coordination on XANES spectra of nanoparticles, this change might be attributed to such an effect. In order to verify this assumption, it is first necessary to obtain information on the orientation of the peptization agent on the nanoparticle surface.

To do so, S K-edge XANES measurements have been performed, whose results are shown in figure 4. Comparing the S K-edge XANES spectrum of the nanoparticles in figure 4 and the spectrum of the pure peptization agent, differences are observed: the white line is split and the position of the shape resonances changes completely. To understand these effects,

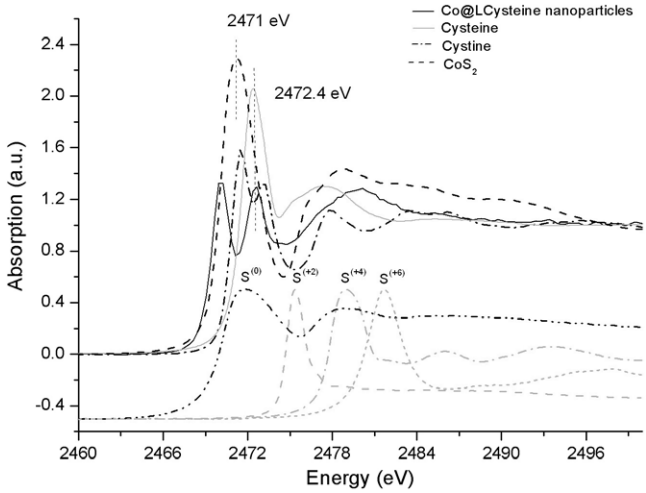

Figure 4. S K-edge XANES spectra of Co nanoparticles peptized by L-cysteine ethyl ester (black solid line) in comparison with reference compounds. Peptization agent L-cysteine ethyl ester (grey solid line), cystine (black dash–dot line), CoS_2 (black dashed line), sulfur (black dash–dot–dot line, lower panel), $(CH_3)SO$ (grey dashed line, lower panel), $(CH_3)SO_2$ (grey dash–dot line, lower panel), $ZnSO_4$ (grey short dashed line, lower panel).

one has to recall that in the XANES spectrum of low-Z elements life time broadening is sufficiently small—in the case of S K-edge spectra only 0.59 eV—to identify transitions into individual molecular orbitals quite easily. This is verified readily when looking at the cystine reference spectrum also displayed in figure 4: in this spectrum, an S–S σ-bond and an S–C σ-bond are expected, which can be directly correlated to the split white line in the cystine spectrum. In fact, the only reason why in the cysteine spectrum only one resonance appears to contribute to the white line is the high similarity of the typical energy positions at which the S–C and the S–H sigma bonds typically occur [49]. More detailed information on the correlation between molecular orbitals/bond characteristics and changes in the white line, partly supported by quantum chemical calculations, can be found in the literature [50–52].

Returning to the spectrum of interest, the spectacular shift to lower energy which is observed in the nanoparticle spectra can be assigned to the formation of a sulfur–metal bond, leading to a notable charge transfer towards the sulfur atom. This interpretation is supported by the CoS_2 spectrum and reference spectra with systematic variation of the formal valency of S shown at the bottom of figure 4, whose energy position can be used as an approximate *scale* on which the formal valency of the absorber atom in a given compound can be determined, as detailed for example in [52–54]. In fact, this observation is suited to provide an explanation for the observed changes in the position of the absorption edge in the Co K-edge spectra of the nanoparticles peptized using L-cysteine ethyl ester, as such a charge transfer should lead to a global chemical shift in a metallic particle.

As the position of the second peak near the onset of the absorption edge remains quite similar to the one of the precursor material, at first sight it might appear unclear whether the second peak corresponds to an S–C bond contribution like in the cystine spectrum, only with a slight shift towards lower energy caused by Co–S bond formation, or whether there are residues of unreacted surfactant, as the energy position of those peak matches very well with the one of L-cysteine. In the latter scenario, however, the corresponding influence of the shape resonances of potential unreacted peptization agent should be observable in the XANES spectra of the

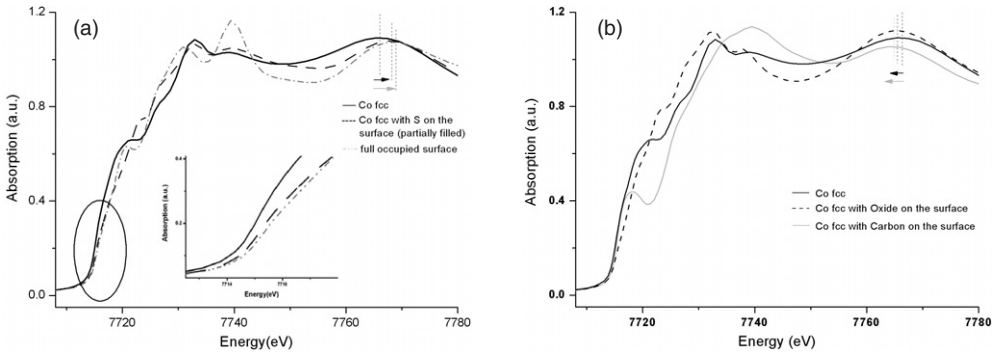

Figure 5. (a) Co K-edge theoretical XANES spectra: Co fcc (black solid line), Co with S on the surface, partially occupied (black dashed line), Co with S on the surface, fully occupied (grey dash–dot–dot line). (b) Co K edge theoretical XANES spectra: Co fcc (black solid line), Co with C on the surface (grey solid line), Co with O on the surface (black dashed line).

particles, for which hardly any evidence is found in the spectra. Therefore, it is likely that the cysteine group remains intact. The fact that the amino acid remains free and intact was also confirmed by infrared spectra [25].

Using the information that sulfur is coordinated to metal obtained at the S K-edge, it is now possible to construct a structural model of the Co–S interface and check whether such a model will be suited to explain the changes observed in the Co K-edge XANES spectrum of the peptized nanoparticle by real-space full multiple scattering calculations using the FEFF8 code [55]. The applicability of this type of calculation for multiple systems including nanoscaled matter has been shown extensively in the literature [56–60].

On account of fcc-like features of nanoparticles observed at the Co K-edge and typical *hollow* positions of sulfur in sulfur–metal compounds [61, 62], the model was built based on a CoS_2 structure [61] in which the disulfide bond was omitted. First, the main features of Co K-edge fcc XANES spectra were reproduced considering a cluster of fcc unit cells up to 10 Å in diameter of only Co atoms, and S atoms were discarded.

Furthermore, to imitate the Co–S interface effect, the first Co–S coordination shell was formed by translation of sulfur top atoms along the Y axis 1.6 Å above the Co surface, so that the typical Co–S distance would be 2.32 Å [61] and inner S atoms remained discarded. All calculations were performed using the spherical self-consistent muffin-tin potential. A core–hole is included on the absorber atom in order to mimic the final state of the photon absorption process. The self-consistent field radius was chosen as 4.189 Å, so that approximately 30 atoms were included in the calculations of potential field. Figure 5(a) confirms the shift of the absorption edge and the shape resonance to slightly higher energy discussed above and illustrates its dependence on sulfur occupation of the cobalt surface. The significance of this result is underlined by the fact that the reproduction of this shift using O or C as surface coordination fails, as shown in figure 5(b).

Amino-functionalization, for example, by L-cysteine ethyl ester, of these metallic Co and FeCo particles provides a good basis for further direct attachment of bioactive molecules or for building up dendrimers, and thus increasing the amount of available amino surface functionalities.

3.2.2. Dextran coating of Co nanoparticles. Dextran is a polysaccharide $(C_6H_{10}O_5)_n$ of anhydroglycose, having mainly 1–6 linkages with some 1–3 linkages at branching points. It has many advantages such as being biocompatible and bioactive. Recent studies, for example,

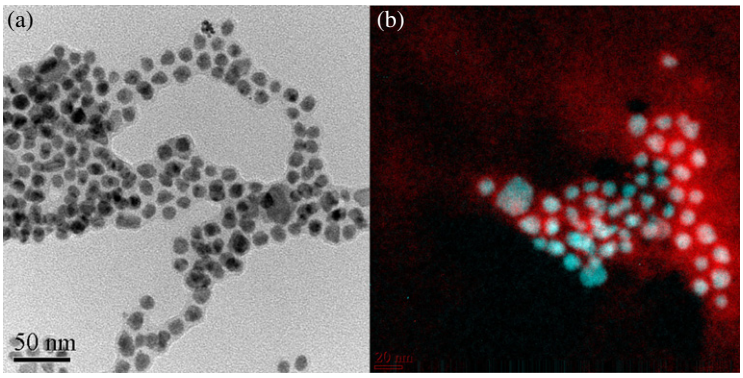

Figure 6. (a) TEM image showing Co nanoparticles coated by dextran (MW 10 000). (b) EFTEM image of carbomethoxydextran coated Co nanoparticles (cobalt (Co $L_{2,3}$ edge, white (blue) spheres) and oxygen (O K edge, as indicated by a diffuse grey (red) colour around the Co nanoparticles).
(This figure is in colour only in the electronic version)

suggested that a dextran coating should be biocompatible because it mimics the glycocalx on cell surfaces [63]. Moreover, dextran coated materials do not degrade enzymatically in most tissues because dextranase, the enzyme that degrades dextran, is produced by bacteria and not by tissues [64]. Its chemical properties include its hydrophilic character as well as its polyhydroxy (OH–) groups. In aqueous solution, dextran interacts with iron oxide particles and covers their surface yielding small aggregates [65–67]. Dextran coated magnetic particles are interesting, for example, as a base material for *in vitro* biomedical applications as magnetic carriers or *in vivo* applications such as MRI. We address the dextran coating of magnetic metal nanoparticles. Co and FeCo particles could be coated by dextran (MW 10 000) and carbomethoxydextran. TEM images display Co nanoparticle agglomerates which are coated by a dextran layer (figure 6(a)). The dextran layer is revealed as a weak contrast in TEM. Figure 6(b) shows the results taken with EFTEM using the Co $L_{2,3}$ and the O K edge. Co particles are represented by a blue colour; oxygen present in the carbomethoxydextran coating is indicated by a diffuse red colour.

These dextran coated Co and FeCo particles have already been tested for cell separation and they show promising results.

3.2.3. SiO_2-coating of Co nanoparticles. It has been demonstrated that the formation of a passive coating with inert materials such as silica on the surface of magnetic particles should not only provide chemical stability to the nanoparticles but also allows covalent binding of various biological ligands for biomedical applications. The silica coating reveals numerous surface silanol groups that can easily react with silane coupling agents, for example, 3-aminopropyl silane (APS), to provide an ideal anchorage for covalent binding of specific ligands. Such a capability potentially allows the future design and the synthesis of magnetic carriers and tags that can be used, for example, for cell separation or to deliver specific ligands to target organs. Depending on the potential area of application, magnetic SiO_2 microspheres, 50 nm to 1 μm in size (e.g. for cell separation) or SiO_2 coated nanoparticles, 10–100 nm size, which are able to penetrate small capillaries within the body tissue (e.g. for drug targeting) are desired.

Co nanoparticles can be coated by a thin SiO_2 layer by a method related to the well-known Stöber process [68], in which silica is formed *in situ* through the base-catalysed hydrolysis and condensation of a sol–gel precursor. This method was applied by a number

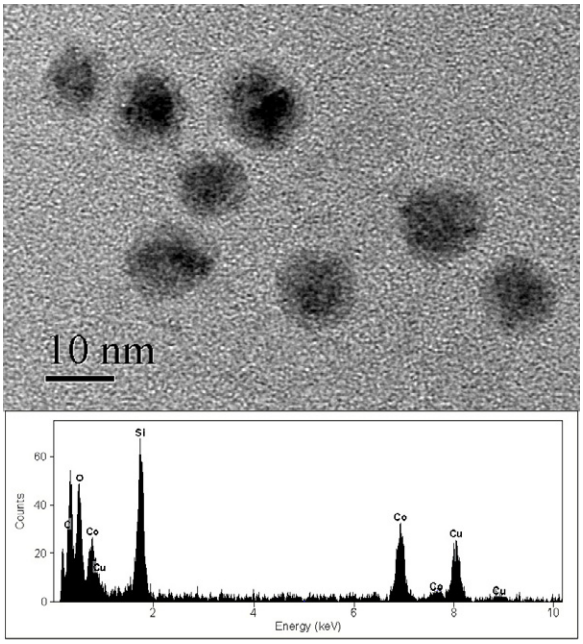

Figure 7. TEM image of pre-stabilized Co nanoparticles whose surfaces have been coated with a thin silica shell (sample Co@SiO_2-2) and EDX spectrum (supporting TEM grid: Cu).

of research groups to coat single iron oxide and cobalt ferrite nanoparticles [69–73] and was extended recently to form silica shells on nanoparticles of noble metals such as silver and gold [74–77]. However, compared to these noble metals, Co is more easily oxidized under the reaction conditions (free heat of formation, e.g., Ag_2O −31.1 kJ mol^{-1}, CoO −237.9 kJ mol^{-1}, Co_3O_4 −891.0 kJ mol^{-1}).

Pre-stabilized Co particles were usually peptized by a surfactant, for example, oleic acid (sample Co@SiO_2-1, details see experiment), to form a stable MF in toluene, but also suspensions of unpeptized, *pre-stabilized* particles were used for silica coating. These particles could be directly coated with amorphous silica, produced via the hydrolysis of TEOS. The surface of the Co particles exhibited an affinity toward silica, in contrast to metallic Au and Ag particles where a primer was typically applied to promote deposition and adhesion of silica on the metal particles. After separation and extensive washing with ethanol, the silica coated particles form colloidal solutions in ethanol. As shown for sample 2, the use of ammonia seemed not to be necessary to form a very thin silica shell around the particles, avoiding complexation and oxidation reactions with the Co core [78]. TEM analysis shows the Co core of the particles (*pre-stabilized* by a thin cobalt oxide shell) which is coated by a thin silica layer (figure 7). EFTEM analysis shows the Co particle core and a Si and O rich silica shell (figure 8).

The Co@SiO_2 nanoparticle size was calculated from TEM images to be around 13 nm, with about 9 nm diameter *pre-stabilized* Co core and about 2 nm silica shell (sample Co@SiO_2-2), and 17 nm, with about 10 nm pre-stabilized Co core and 3.5 nm silica shell (sample Co@SiO_2-1). Note that the silica shell was homogeneous on each individual particle. The IR spectra show characteristic bands of alkyl chains at 2854–2966 cm^{-1}, suggesting unhydrolysed ethoxy groups remaining at the particle surface. The broad band at 1052 cm^{-1} is characteristic for Si–O–Si bonding.

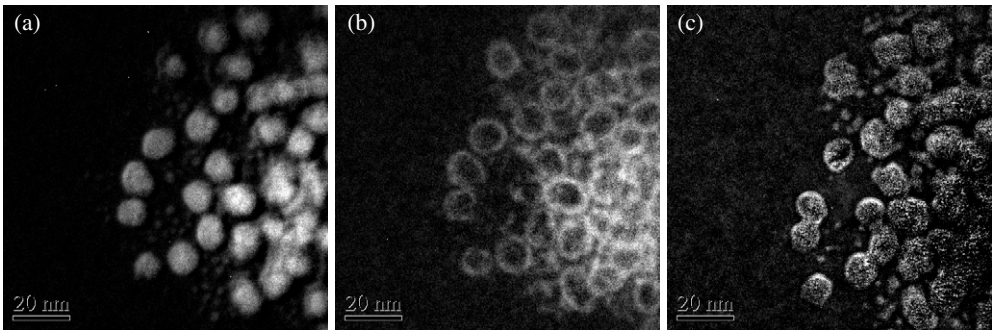

Figure 8. EFTEM images of $Co@SiO_2$ nanoparticles: cobalt mapping (Co $L_{2,3}$ edge) (a) and oxygen mapping (O K edge) (b), and Si mapping (Si $L_{2,3}$ edge) (c) (sample $Co@SiO_2$-1).

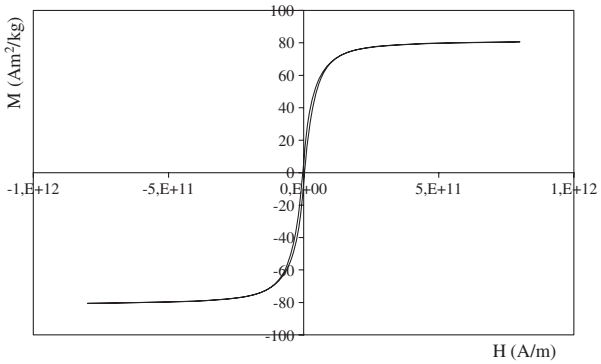

Figure 9. Magnetization curve of $Co@SiO_2$ particles (sample $Co@SiO_2$-2) obtained by AGM at room temperature.

Magnetic characterization of the silica coated Co particles ($Co@SiO_2$) was performed at room temperature employing an alternating gradient magnetometer (AGM). As an example, figure 9 shows the magnetization curve of sample $Co@SiO_2$-2. It should be stressed that these are raw data, in which the magnetization is expressed in A m^2 kg^{-1} powder, including the diamagnetic SiO_2 shell and the passivating cobalt oxide layer. This contributes to the observed discrepancy to the saturation magnetization for fcc Co bulk material (162 A m^2 kg^{-1} [79]). Moreover, it has been observed that the smaller the particle size, the greater is the surface contribution and the total decrease in saturation magnetization [78, 80].

$Co@SiO_2$ particles originating from Co nanoparticles peptized by oleic acid (sample $Co@SiO_2$-1) exhibited an initial saturation magnetization M_s of 34 A m^2 kg^{-1}. When unpeptized, *pre-stabilized* Co particles were employed for synthesis of $Co@SiO_2$ (sample $Co@SiO_2$-2), the initial saturation magnetization M_s was 80 A m^2 kg^{-1}, which was comparable to that of the applied, *pre-stabilized* Co nanoparticles. This increase in magnetization can be partially attributed to a higher Co content of the samples (around 70 wt% Co versus 50 wt% Co in the previous case, according to atomic emission spectroscopy with inductively coupled plasma (AES-ICP)) and, moreover, to a smaller cobalt oxide layer around the metallic Co core. $Co@SiO_2$ particles (sample $Co@SiO_2$-2) were stable in water for at least 1 month. Preliminary experiments for amino-functionalization with APS were successful (1.3% N; as determined by elemental analysis).

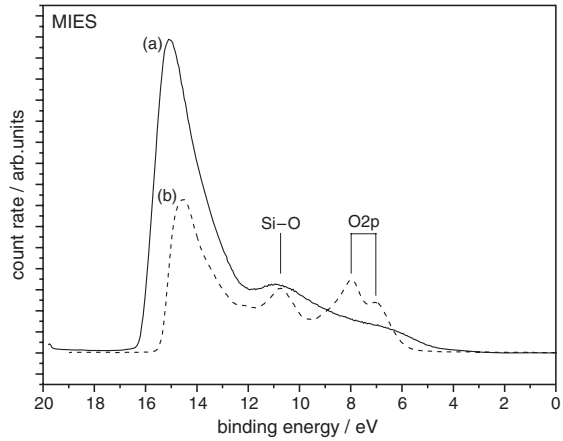

Figure 10. MIES spectra for (a) $Co@SiO_2$ nanoparticles (sample $Co@SiO_2$-2), and (b) low-defect SiO_2 films on Mo(112) [81] (see text for discussion of spectral features of Si–O and O 2p).

The combination of electron spectroscopic techniques provides detailed information on the structure of the silica coated Co particles which will be demonstrated for the samples $Co@SiO_2$-1 and -2. MIES, in combination with UPS (HeI), provides information on the electronic structure of the coating layer: since the information depth is zero for MIES and less than 1 nm for UPS, there is no interference from the Co particles of the core in the spectra. The analysis of the MIES and UPS spectra can be based on the comparison with *fingerprint* spectra of SiO_2 (see [81] for recent data, combining MIES and UPS). It should, however, be noted that electron spectroscopy on nanoparticles in general is considerably more difficult because the micro-roughness of the sample affects the angular distribution of the emitted electrons in such a manner that the emission intensity available for spectral analysis is reduced by one order of magnitude as compared to that from the corresponding films.

The MIES data (a) (figure 10) show considerable similarity with the above-mentioned *fingerprint* spectra (b) in as much as both display structures around binding energies of 7.5 eV (O 2p) and 11 eV (Si–O). O 2p is due to the nonbonding O 2p states while Si–O is related to a σ- type Si–O bonding state. On the other hand, clear differences in details between the spectra are obvious. Moreover, the UPS spectra (not shown) are rather different from the available *fingerprint* spectra for SiO_2. Obviously, the coating film is so thin that the UPS spectra mirror the interaction of Si, O, and Co in the interface region. We conclude that the Co particles are coated by an insulating film (band gap: 6.4 eV) which contains both Si and oxygen, but, at least in the interface region to the Co core, is not simply SiO_2. On the basis of a comparison with available fingerprint spectra for Co and CoO films [82] and judging from the fact that no emission from the core can be seen in the band gap region (for binding energies 0–4 eV), the coating film, within our detection limits, covers the Co particle's surface completely. As was pointed above, the oxidation kinetics of Co films is complicated [42], and probably depends sensitively on the particle size.

Co oxides, films, and overlayers in particular, have been widely studied by XPS because of their importance as catalysts for complete oxidation [83]. Consequently, the characterization of the Co charge state has been considered as an important issue. Related to this, and of importance for the present study, extensive work has been done on the oxidation of metallic Co films [79, 84]. The fact that *fingerprint* spectra are available, both for Co and CoO, facilitates the interpretation of the Al Kα spectra in the 2p Co region, shown in figure 11 as a function

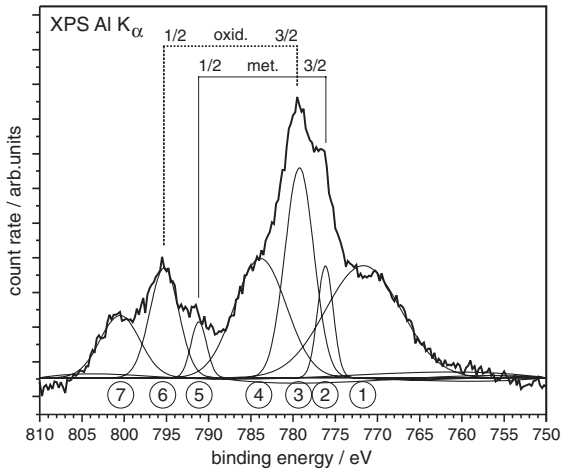

Figure 11. XPS spectra for Co@SiO_2 nanoparticles (sample Co@SiO_2-2). The brackets denote the positions of the emission from the Co 2p fine structure states in oxidic and metallic Co, respectively (see text for detailed discussion of spectral feature (1)–(7)).

of the binding energy of the emitted electrons for sample Co@SiO_2-2. We notice several structures, two peaks, accompanied by various shoulders, in the Co 2p region. On the basis of previous results on Co and CoO films [83, 84], the two peaks (peak (3) and (6) at 779.1 and 795.2 eV, respectively) must be attributed to Co $2p_{3/2}$ and Co $2p_{1/2}$ in CoO originating from the smooth oxidation. The satellites associated with these peaks on the high-binding energy side ((4) and (7)) are due to multi-electron effects; for their description the Co 3d–O 2p coupling needs to be taken into account [85, 86]. The fine structure splitting of the Co $2p_{3/2}$ and Co $2p_{1/2}$ components is 16.1 eV, indicative for Co^{2+} ions (as expected for CoO); for Co^{3+} (as in Co_3O_4) the splitting would be around 15.1 eV, and the shake-up structures would be much less pronounced [83, 87].

Two shoulders are seen in the slopes of the oxidic Co $2p_{3/2}$ and Co $2p_{1/2}$ peaks on their low-energy sides ((2) and (5)); these are due to the $2p_{3/2}$ and $2p_{1/2}$ emission from metallic Co. The broad shoulder (1), centred around 770 eV, is due to the Auger LMM process.

A Shirley background was subtracted from the transmission corrected XPS spectra before starting the fitting procedure shown in figure 11, in which we have included all above-mentioned spectral features. The two peaks representing the Co 2p fine structure states in Co^0 (metallic cobalt) were positioned at 776.1 and 791.1 eV for Co $2p_{3/2}$ and Co $2p_{1/2}$, respectively [84]. The result of the fitting indicates that metallic Co contributes about 20% to the Co emission displayed in figure 11. This contribution of Co^0 to the Co 2p emission structure is compatible with the shell structure suggested by TEM (see above), considering the fact that the sampling depth of XPS is of the order of 3–5 nm (mean free path of the ejected electron about 2 nm at about 700 eV). For sample Co@SiO_2-2 XPS measurements were carried out over an extended period of time, and indicate that the particles kept under air at room temperature are stable over weeks. Summarizing, in the present case, the core level spectroscopy allows for a sensitive test of the charge state of the Co species, being not only able to distinguish between metallic and oxidic Co, but also between different oxidation states.

Besides SiO_2 coated nanoparticles, silica microspheres containing embedded magnetic Co particles were prepared by a two-step procedure: firstly, *pre-stabilized* Co nanoparticles were suspended in water and reacted with 3-aminopropylsilane and active silica (Na_3SiO_3). In a

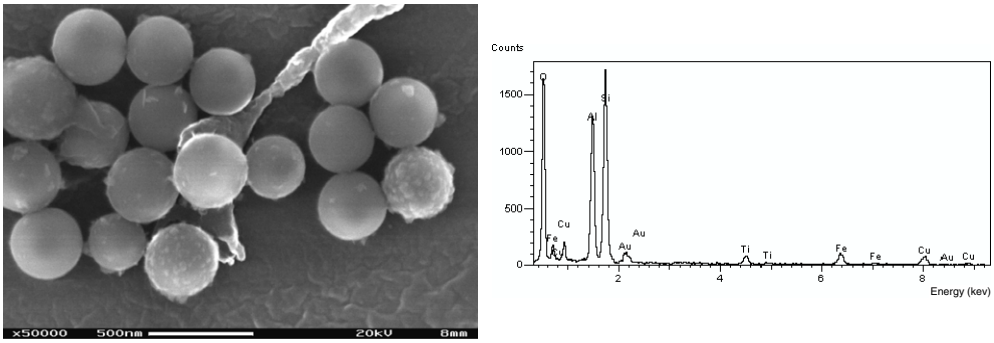

Figure 12. SEM image displaying several magnetic SiO_2 microspheres prepared from Fe nanoparticles and corresponding EDX spectrum (supporting TEM grid: Cu; sample holder: Al, Au, Ti).

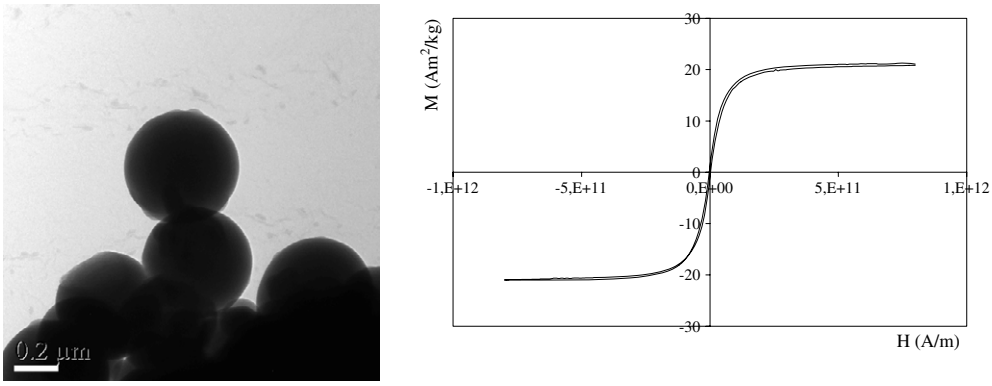

Figure 13. TEM image showing magnetic SiO_2 microspheres prepared from Co nanoparticles and magnetization curve (24.4 wt% Co).

second step TEOS and NH_4OH were added and stirred for 24 h at room temperature. The resulting magnetic SiO_2 microspheres were quite uniform with a diameter of around 330 and 520 nm for embedded Fe and Co particles, respectively (figures 12 and 13).

3.2.4. Polymer microspheres. Magnetic functional polymer microspheres can be easily collected with the application of a magnetic field and provide, after coupling to appropriate ligands, an effective tool to achieve rapid, simple, and specific biological separation such as cell isolation, protein purification, and immunoassay. Iron oxide particles have been encapsulated into polymer microspheres by applying, for example, conventional emulsion polymerization [88], dispersion polymerization [89, 90], suspension polymerization [91], and seed polymerization [92]. Magnetic Co particles were encapsulated in poly(methylmetacrylate-divinylbenzene) microspheres by suspension polymerization, resulting in spheres with a diameter of about 15 μm. PVA was employed as a stabilizer in the aqueous solution to stabilize the droplets. The Co particles were peptized with a hydrophobic KorantinSH shell which could be easily mixed with the organic mixture of MMA, DVB and the initiator to form a uniform oil phase. Figure 14 displays several magnetic microspheres and the magnetization curve.

The saturation magnetization was found to be 33 A m^2 kg^{-1}, which is higher than those reported in similar work with Fe_3O_4 magnetic fluid [91].

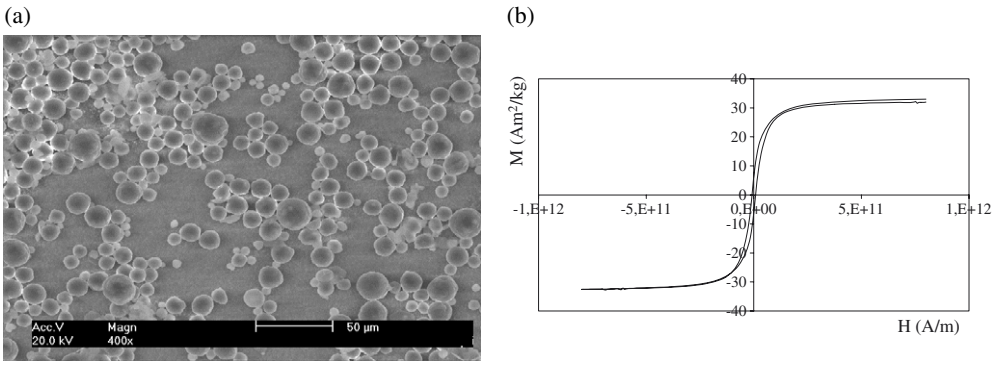

Figure 14. (a) SEM micrograph showing Co nanoparticles embedded into poly(MMA-DVB) microspheres. (b) Magnetization curve (35 wt% Co).

4. Conclusion

Air-stable magnetic metal particles were prepared via thermolysis of the corresponding metal carbonyls in the presence of aluminium alkyls, followed by careful surface passivation. Co, Fe, and FeCo nanoparticles were obtained by this approach. We have developed several procedures for modifying the surface chemistry of the metallic Co nanoparticles, for example, by functionalization with L-cysteine ethyl ester, dextran, and silica coating, as well as embedding the particles into silica or polymer microspheres. These modifications will allow future binding of bioactive molecules for biomedical applications.

Acknowledgments

This work was supported by Deutsche Forschungsgemeinschaft (DFG), priority program SPP 1104 'Kolloidale magnetische Flüssigkeiten'.

References

[1] Odenbach S 2002 *Ferrofluids* (Heidelberg: Springer)
[2] Papell S S 1965 *US Patent Specification* 3 215 572
[3] Khalafalla S E and Reimers G W 1973 *US Patent Specification* 3 764 540
[4] Berkovsky B M, Medvedev V F and Krakov M S 1993 *Magnetic Fluids—Engineering Applications* (Oxford: Oxford University Press)
[5] Mornet S, Vasseur S, Grasset F and Duguet E 2004 *J. Mater. Chem.* **14** 2161
[6] Santos J G, Silveira L, Gansau G, Buske N and Morais P 2004 *J. Magn. Magn. Mater.* **272** 2330
[7] Lacava L, Garcia V, Kuckelhaus S, Azevedo R, Lacava Z, Silva O, Pelegrini F, Gansau C, Buske N and Morais P 2003 *J. Appl. Phys.* **93** 7563
[8] Tedesco A, Oliveira D, Lacava Z, Azevedo R, Lima E, Gansau C, Buske N and Morais P 2003 *J. Appl. Phys.* **93** 6704
[9] Caruso F 2001 *Adv. Mater.* **13** 11
[10] Katz E and Willner I 2004 *Angew. Chem. Int. Edn* **43** 6042
[11] Dinega D and Bawendi M G 1999 *Angew. Chem. Int. Edn* **38** 1788
[12] Puntes V F, Krishnan K M and Alivisatos P 2001 *Appl. Phys. Lett.* **78** 2187
[13] Giersig M and Hilgendorff M 1999 *J. Phys. D: Appl. Phys.* **32** L111
[14] Wiedwald U, Spasova M, Salabas E L, Ulmeanu M and Farle M 2003 *Phys. Rev.* B **68** 064424
[15] Ying Y, Rioux R M, Erdonmez C K, Hughes S, Somorjai G and Alivisatos P 2004 *Science* **304** 711
[16] Papirer E, Horny P, Balard H, Anthore R, Petipas C and Martinet A 1983 *J. Colloid Interface Sci.* **94** 207
[17] Papirer E, Horny P, Balard H, Anthore R, Petipas C and Martinet A 1983 *J. Colloid Interface Sci.* **94** 220
[18] Park S J, Kim S, Lee S, Khim Z, Char K and Hyeon T J 2000 *Am. Chem. Soc.* **122** 8581

[19] Burke N, Stöver H and Dawson F 2002 *Chem. Mater.* **14** 4752
[20] Butter K, Philipse A P and Vroege G J 2002 *J. Magn. Magn. Mater.* **252** 1
[21] Zubris M, King R B, Garmestani H and Tannenbaum R 2005 *J. Mater. Chem.* **15** 1277
[22] Hütten A, Sudfeld D, Ennen I, Reiss G, Wojczykowski K and Jutzi P 2005 *J. Magn. Magn. Mater.* **293** 93
[23] Bönnemann H, Brijoux W, Brinkmann R, Matoussevitch N, Waldöfner N, Palina N and Modrow H 2003 *Inorg. Chim. Acta* **350** 617
[24] Bönnemann H *et al* 2005 *Appl. Organomet. Chem.* **19** 790
[25] Behrens S *et al* 2006 *Z. Phys. Chem.* **220** 3
[26] Harada Y, Masuda S and Ozaki H 1997 *Chem. Rev.* **97** 1897
[27] Morgner H 2000 *Adv. At. Mol. Opt. Phys.* **42** 387
[28] Dieckhoff S, Schlett V, Possart W, Hennemann O D, Günster J and Kempter V 1996 *Appl. Surf. Sci.* **103** 221
[29] Ochs D, Brause M, Maus-Friedrichs W, Kempter V, Puchin V, Shluger A and Kantorovich L 1996 *Surf. Sci.* **365** 557
[30] Kantorovich L, Shluger A L, Sushko P V, Günster J, Stracke P, Goodman D W and Kempter V 1999 *Faraday Discuss.* **114** 173
[31] Annual Report CAMD 2005 www.camd.lsu.edu
[32] Lemonnier M, Collet O, Depautex C, Esteva J M and Raoux R 1978 *Nucl. Instrum. Methods* A **152** 109
[33] Thompson A 2001 Electron binding energies *X-ray Data Booklet* (Berkeley, CA: Lawrence Berkeley National Laboratory, University of California)
[34] http://ixs.iit.edu/subcommittee_reports/sc/SC00report.pdf
[35] http://ixs.iit.edu/subcommittee_reports/sc/err-rep.pdf
[36] Ressler T 1997 *J. Physique* IV **7** 2
[37] Bucher S, Hormes J, Modrow H, Brinkmann R, Waldöfner N, Bönnemann H, Beuermann L, Krischok S, Maus-Friedrichs W and Kempter V 2002 *Surf. Sci.* **497** 321
[38] Modrow H, Bucher S, Hormes J, Brinkmann R and Bönnemann H 2003 *J. Phys. Chem.* B **107** 3684
[39] Wen F *et al* 2005 *Eur. J. Inorg. Chem.* **18** 3625
[40] Odenbach S (ed) 2006 Synthesis and characterization *Magnetic Fluids* (*Springer Lecture Notes in Physics*) (Berlin: Springer) at press
[41] Rudenkiy S *et al* 2004 *Appl. Organomet. Chem.* **18** 553
[42] Smardz L, Köbler U and Zinn W 1992 *J. Appl. Phys.* **71** 5199
[43] Margeat O, Amiens C, Chaudret B, Lecante P and Benfield R E 2005 *Chem. Mater.* **17** 107
[44] Zhang P and Sham T K 2003 *Phys. Rev. Lett.* **90** 245502
[45] Vestal C R and Zhang Z J 2003 *J. Am. Chem. Soc.* **125** 9828
[46] Modrow H 2004 *Appl. Spectrosc. Rev.* **39** 183
[47] Skumryev V, Stoyanov S, Zhang Y, Hadjipanayis G, Givord D and Nogues J 2003 *Nature* **19** 850
[48] Song Y, Modrow H, Henry L L, Saw C K, Doomes E E, Palshin V, Hormes J and Kumar C S S R 2006 *Chem. Mater.* **18** 2817
[49] Prange A, Dahl C, Trüper H G, Behnke M, Hahn J, Modrow H and Hormes J 2002 *Eur. Phys. J.* D **20** 589
[50] Chauvistre R, Hormes J, Hartmann E, Etzenbach N, Hosch R and Hahn J 1997 *J. Chem. Phys.* **223** 293
[51] Flemming B, Modrow H, Hallmeier K H, Hormes J, Reinhold J and Szargan R 2001 *Chem. Phys.* **270** 405
[52] von Busch F, Hormes J, Modrow H and Nestmann N B 2003 Interaction of atomic core electrons with the molecular valence shell *Interactions in Molecules—Electronic and Steric Effects* ed S D Peyerimhoff (New York: Wiley–VCH) pp 193–257 (ISBN: 3-527-27732-3)
[53] Vairavamurthy A, Zhou W, Eglinton T and Manowitz B 1994 *Geochim. Cosmochim. Acta* **71** 520
[54] Pantelouris A, Modrow H, Pantelouris M, Hormes J and Reinen D 2004 *Chem. Phys.* **300** 13
[55] Ankudinov A L, Ravel B, Rehr J J and Conradson S D 1998 *Phys. Rev.* B **58** 7565
[56] Modrow H, Bucher S, Rehr J J and Ankudinov A 2003 *Phys. Rev.* B **67** 035123
[57] Gilbert B, Frazer B H, Belz A, Conrad P G, Nealson K H, Haskel D, Lang J C and de Stasi G 2003 *J. Phys. Chem.* A **107** 2839
[58] Kravtsova A N, Stekhin I E, Soldatov A V, Liu X and Fleet M E 2004 *Phys. Rev.* B **69** 134109
[59] Reich A, Panthöfer M, Modrow H, Wedig U and Jansen M 2004 *J. Am. Chem. Soc.* **126** 14428
[60] Angermund K *et al* 2003 *J. Phys. Chem.* B **107** 7507
[61] Nowack E, Schwarzenbach D and Hahn T 1991 *Acta Crystallogr.* B **47** 650
[62] Will G, Lauterjung J, Schmitz H and Hinze E 1984 *Mater. Res. Soc. Symp. Proc.* **22** 49
[63] Holland N B, Qiu Y X, Ruegsegger M and Marchant R E 1998 *Nature* **392** 477
[64] Crepon B, Chytry J J and Kopeček R 1991 *Biomaterials* **12** 550
[65] Bautista M C, Bomati-Miguel O, del Puerto Morales M, Serna C J and Veintemillas-Verdaguer S 2005 *J. Magn. Magn. Mater.* **293** 20

[66] Xia Z, Wang G, Kaixiong T and Li J 2005 *J. Magn. Magn. Mater.* **293** 182
[67] Mornet S, Portier J and Duguet E 2005 *J. Magn. Magn. Mater.* **293** 127
[68] Stöber W, Fink A and Bohn E 1968 *J. Colloid Interface Sci.* **26** 62
[69] Lu Y, Yin Y, Mayers B and Xia Y 2002 *Nano Lett.* **2** 183
[70] Autenrieth T, Wagner J, Hempelmann R, Härtl W, Robert A and Grübel G 2004 *Appl. Organomet. Chem.* **18** 520
[71] Wagner J, Autenrieth T and Hempelmann R 2002 *J. Magn. Magn. Mater.* **252** 4
[72] Philipse A P, van Bruggen M P B and Pathmamanoharan C 1994 *Langmuir* **10** 92
[73] Woo K, Hong J and Ahn J P 2005 *J. Magn. Magn. Mater.* **293** 177
[74] Liz-Marzan L M, Giersig M and Mulvaney P 1996 *Chem. Commun.* 731
[75] Kobayashi Y, Katakami H, Mine E, Nagao D, Konno M and Liz-Marzan L 2005 *J. Colloid Interface Sci.* **283** 392
[76] Liz-Marzan L M, Giersig M and Mulvaney P 1996 *Langmuir* **12** 4329
[77] Hall S R, Davis S A and Mann S 2000 *Langmuir* **16** 1454
[78] Kobayashi Y, Horie M, Konno M, Rodriguez-Gonzáles B and Liz-Marzán L M 2003 *J. Phys. Chem.* B **107** 7420
[79] Bozorth R M 1951 *Ferromagnetism* (New York: Van Nostrand)
[80] Petit C, Taleb A and Pileni M P 1999 *J. Phys. Chem.* B **103** 1805
[81] Wendt S, Frerichs M, Wie T, Chen M S, Kempter V and Goodman D W 2004 *Surf. Sci.* **565** 107
[82] Frerichs M, Schweiger F X, Voigts F, Rudenkiy S, Maus-Friedrichs W and Kempter V 2005 *Surf. Interface Anal.* **37** 633
[83] Jimenez V M, Espinos J P and Gonzalez-Elipe A R 1998 *Surf. Interface Anal.* **26** 62
[84] Kim K S 1974 *Phys. Rev.* B **11** 2177
[85] Okada K and Kotani A 1992 *J. Phys. Soc. Japan* **61** 449
[86] Lee G and Oh S 1991 *Phys. Rev.* B **43** 14674
[87] Mekki A, Holland D, Ziq Kh and McConville C F 1997 *J. Non-Cryst. Solids* **220** 267
[88] Ramírez L P and Landfester K 2003 *Macromol. Chem. Phys.* **204** 22
[89] Li X H and Sun Z H 1995 *J. Appl. Polym. Sci.* **89** 2058
[90] Horák D, Bohácek L and Šubrt M 2000 *J. Polym. Sci.* A **58** 1161
[91] Yang C, Liu H, Guan Y, Xing J, Liu J and Shan G 2005 *J. Magn. Magn. Mater.* **293** 187
[92] Lee J and Senna M 1995 *Colloid Polym. Sci.* **273** 76